NanoMatEn 2015 International Conference Proceeding

http://www.setcor.org/conferences/Nano-MatEn-2015

The Effect of pH on Expanding Titanate Nanotubes & Their Use as a High Capacity Lithium-Ion Battery Electrode with High Rate Capability

A. Yürüm[1,*], M. Yarali[2], E. Bicer[3], S. Alkan Gürsel[2]

[1]Sabanci University Nanotechnology Research and Application Center, Istanbul, Turkey
[2]Faculty of Engineering and Natural Sciences, Sabanci University, Istanbul, Turkey
[3]Faculty of Pharmacy, Yeni Yuzyil University, Istanbul, Turkey

Abstract: Improvement of lithium-ion electrodes with high charge and discharge capacities is in high need especially for electronic devices and electric vehicles (Gong *et al*., 2013). For that reaso, development of ion transport in the crystal structure is needed (Li *et al*., 2013). The general idea is synthesizing nanometer scale particles. Reducing the particle size helps the ion diffusion in the structure (He *et al*., 2014). Titanate nanotubes are promising materials because of their special morphology and high specific surface area. The nanotubes are formed by rolling-up of titanate nanosheets (Kasuga *et al*., 1998). These titanates provide high rate capability and low volume expansion upon lithiation (Ren *et al*., 2010). More importantly their tubular structure helps the transport of ions through the crystal. In this study, we synthesized titanate nanotubes and modified the interlayer distance by changing the pH. For the characterization XRD (Figure 1), SEM (Figure 2) and BET (Figure 3) techniques were used. In addition, the effect of interlayer distance on energy capacity and rate capability was investigated. The shortest interlayer distance was observed at pH 4,5. Getting further away from this point, interlayer distances increased and this also increased the nanotube diameter. Conversely, specific surface area reaches its maximum value at pH 4,5. Potential-capacity profiles of TiO_2 nanoparticles showed distinct potential plateaus. Nevertheless, a very fast capacity drop was observed for TiO_2 particles. On the other hand, for titanates, broad peaks appear in CV measurements. For titanates capacities higher than 700 mAh/g were obtained. More importantly, titanates showed exceptional rate capabilities especially at wider interlayer distances due to higher mobility of ions in the structure (Figure 4). It was found that interlayer distance plays an important role in rate capability. However the material still needs some modifications to stabilize the capacity.

Keywords: expanded titanate nanotubes, pH, high capacity, high rate capability, Li-ion.
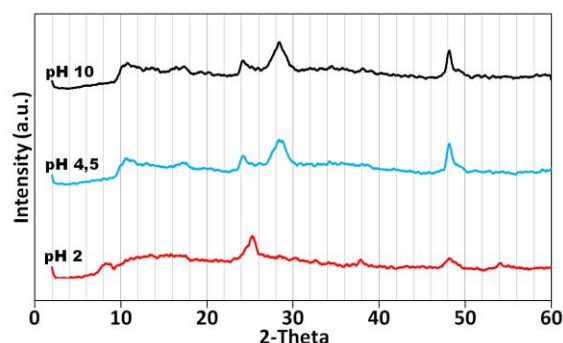
Figure 1: The effect of pH on crystal structure of titanates: the peak around 10º ((200) reflection plane) first shifted to higher degrees. After pH value of 4,5, titanate structure started to transform back to TiO_2 (anatase). From that point, this peaks shifted to lower degrees. (002) reflection plane is related to interlayer distance of titanate nanotubes. This means that the nanotubes first shrink and then expand.
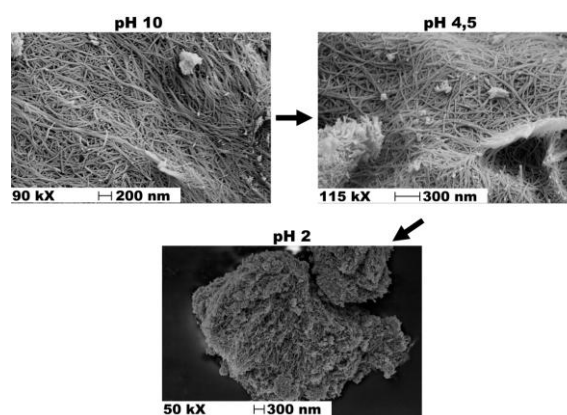

Figure 2: SEM images of titanates after being treated at various pH values: At pH 10, diameter of the nanotubes ranged from 20-35 nm. When pH value dropped to 4,5, the diameter was between 15 and 25 nm. Finally at ph 2, similar to pH 10, the diameter ranges from 20-30 nm. Additionally, at pH values of 10 and 4,5 long nanotubes were observed. However due to structural transformation, at pH 2, the nanotubes got shorter.
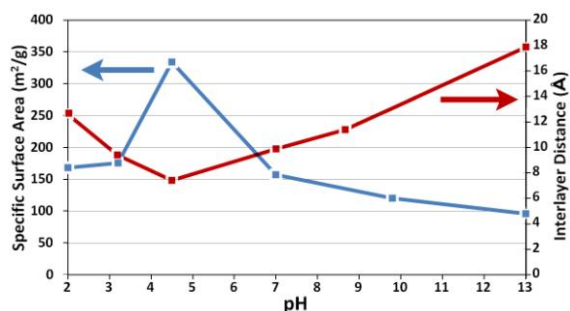
Figure 3: Surface area and interlayer distance values at various pH values: Similar to XRD and SEM results, the shortest interlayer distance of 7,4 Å was observed at pH value of 4,5. Getting further away from this point, interlayer distances increased and this also increased the nanotube diameter. However, the highest specific surface area value of 334 m^2/g at was obtained at pH of 4,5.
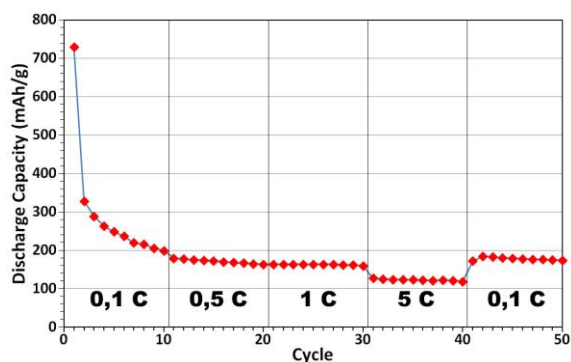

Figure 4: Rate capability test of titanate modified at pH 4,5: Potential-capacity profiles of TiO_2 (anatase) nanoparticles showed distinct potential plateaus at 1.7 and 2.2 V for discharging and charging, respectively. However, the capacity dropped from 254 mAh/g to 87 mAh/g in 10 cycles. Titanates show broad peaks appear in CV measurement, thus no distinct plateau was observed at potential-capacity profile. For titanates capacities as high as 750 mAh/g were obtained. More importantly, titanates showed exceptional rate capabilities especially at wider interlayer distances due to higher mobility of ions in the structure.

References:

Gong , Y. J., Yang, S. B., Liu, Z., Ma, L. L., Vajtai, R., Ajayan, P. M. (2013), Graphene-Network-Backboned Architectures for High-Performance Lithium Storage, *Adv. Mater.*, 25, 3979.

Li, L., Raji, A.-R. O., Tour, J. M. (2013), Graphene-Wrapped MnO_2–Graphene Nanoribbons as Anode Materials for High-Performance Lithium Ion Batteries, *Adv.Mater.*, 25, 6298.

He, M., Kravchyk, K., Walter, M., Kovalenko, M. V. (2014), Monodisperse Antimony Nanocrystals for High-Rate Li-ion and Na-ion Battery Anodes: Nano versus Bulk, *Nano Lett.*, 14, 1255.

Kasuga, T., Hiramatsu, M., Hoson, A., Sekino, T., Niihara, K. (1998), Formation of Titanium Oxide Nanotube, *Langmuir*, 14, 3160.

Ren, Y., Hardwick, L. J., Bruce, P. G. (2010), Lithium Intercalation into Mesoporous Anatase with an Ordered 3D Pore Structure, *Angew. Chem. Int. Ed.*, 49, 2570.

Effect of Preparation Temperature and Immersion Duration on the Ionic Conductivity and Oxygen Permeability of Composite Materials for the use as Gas Separators in Alkaline Water Electrolyzers

J. Stojadinović[1], G. Kasiribidhendi[1], F. La Mantia[1]

[1]University of Bochum, Dept. Chemistry and Biochemistry, Center for Electrochemical Sciences, Bochum, Germany

Abstract

Development of materials for the use in alkaline electrolyzers for gas separation has been directed towards surpassing the ionic conductivity, gas tightness, chemical, mechanical and thermal resistivity, life span, and cost effectiveness of the health hazardous asbestos and current state of the art Zirfon® Perl separator [1,2].

The aim of this study is to gather better understanding of the effect of the materials' preparation process and the immersion duration in 25 wt. % KOH on the ionic conductivity and gas barrier properties. Ionic conductivity of different gas separation membranes can be accurately determined by Electrochemical Impedance Spectroscopy with a four-electrode zero gap cell, while the use of the four-electrode non-zero gap cell coupled with a Mass Spectrometer enables the oxygen permeability assessment [3].

The immersion duration increased the ionic conductivity of the developed material, which was not the case with the other separators used for comparative purposes. The temperature at which the preparation took place was shown to have a significant influence on the ionic conductivity of the developed separators. Understanding of the preparation parameters' interactions enables the optimisation of the material fabrication. Additionally, it contributes towards broadening the material's application to systems other than alkaline electrolyzers, such as fuel cells and solar hydrogen generation.

Keywords: gas separation, temperature, immersion duration, ionic conductivity, oxygen permeability.

Introduction

The manufacturers of alkaline water electrolyzers are still facing the issue of deploying the separator for hydrogen and oxygen, which will enable improved performance of the electrolysis system. An advanced material should fulfill multiple requirements, such as: good gas separation, high ionic conductivity, chemical and thermal stability in highly concentrated KOH solution. Moreover, the mechanical strength is required, taking into account that the industrial alkaline electrolysis separators may be up to 4 m^2 large. Further on, the material should be cost effective, environmentally acceptable, and provide safe operation over the years. Development of a separator possessing such properties is attracting attention of several research groups. Ionic conductivity of the state-of-the-art membrane Zirfon® Perl tailored for this application equals to approx. 160 mS cm^{-1}, as reported by [2]. These relatively low values of ionic conductivity do not facilitate reduction of the electricity consumption during the electrolysis process. Our aim was to develop a material which overcomes the shortcomings of the competitive separators. The material characterization was performed using the methodology developed in-house and explained elsewhere [3].

Experimental

Preparation of a composite material was undertaken at 8, 22 and 40°C to assess the influence of temperature on physical chemical properties of the developed separators. Asbestos samples used in this study were cut from a typical separator for alkaline electrolyzers (chrysotile, $Mg_3Si_2O_5(OH)_4$). Polyphenylene sulphide (PPS) type 306P41 5/5, with an area density of 550 [g m^{-2}] and air permeability of 160 [l dm^{-2} min^{-1}] at 200 Pa, has been supplied by Heimbach Filtration GmbH. The differences in the separators' thicknesses were taken into account for the calculation of conductivity [3].

In this study, 25 wt. % KOH electrolyte, corresponding to the operating electrolyte in industrial alkaline electrolyzers, was used.

All membranes were soaked in this electrolyte prior to measurements by pouring it onto the membrane placed on the ceramic frit and forcing it through the membrane body by a vacuum pump.

For the assessment of the effect of the material preparation temperature on the ionic resistance (and calculated conductivity), the measurements were undertaken three weeks after immersion in the electrolyte. In order to determine the ionic conductivity of the membranes, the ionic resistance

was measured via electrochemical impedance spectroscopy (EIS) in the zero gap electrochemical cell in a galvanostatic mode (Gamry Instruments Reference 600 potentiostat), as explained elsewhere [3]. The cells were filled with 5.5 M KOH (25 wt. %) electrolyte prior to each measurement. The current density of 160 mA cm^{-2} was chosen for the resistance measurements because it ensured the electrolysis regime during the measurements and corresponded to the current density applied in the industrial conditions. Frequencies were swept from 1 KHz to 100 mHz, with the amplitude of 10 mA. Ionic resistance measurements were performed for three separator samples prepared at each temperature and their average calculated ionic conductivity is shown in Fig. 1. Calculations of the ionic conductivity and oxygen permeability are explained in detail elsewhere [3].

For the oxygen permeability determination a non-zero gap cell [3] was used. In situ measurements of the oxygen cross over for different separators were undertaken by coupling the chronopotentiometry method, which provides the desired electrolysis regime, with a quadrupole mass spectrometer, as explained in [3]. For the oxygen permeability measurements two separators were prepared and tested at each temperature (8, 22 and 40°C).

For the assessment of the effect of the immersion duration on the ionic conductivity, the separators were characterized after less than one month and three months immersion (0 and 3 months) in 25 wt. % KOH.

Results and discussion

The ionic conductivity, κ, and oxygen permeability, $y_{O_2}^{ELS}$, change for different preparation temperatures (*Fig. 1*). Similar values were obtained at 22 and 40°C, with the least scattering occurring at 22°C. The values of the ionic conductivity, equal to approx. 280 mS cm^{-1}, and oxygen permeability, equal to approx. 0.08 %, qualify this material to be one of the most advanced separators for the use in alkaline electrolysis.

Influence of the duration of immersion in 25 wt. % KOH on the ionic conductivity, κ, of different separators is shown in *Fig. 2*. Besides possessing the highest initial ionic conductivity, the composite separator exhibits conductivity increase of more than 100 mS cm^{-1} during a 3 months immersion.

Fig. 1 Influence of the preparation temperature on the ionic conductivity, κ, and oxygen permeability, $y_{O_2}^{ELS}$, of developed separator material immersed in KOH for three weeks before the measurements.

Fig. 2 Influence of the duration of immersion in KOH on the ionic conductivity, κ, of different separators.

Conclusions

The developed composite separator possesses significantly higher ionic conductivity compared to the competitive separator materials available on the market, while maintaining similar oxygen permeability. Its ionic conductivity shows a steady increase trend with the longer immersion duration in 25 wt. % KOH. Such properties would enable reduced electricity consumption resulting in the increased efficiency of the alkaline electrolysis process. The initial efficiency, according to these results, would be even enhanced during the operation.

References

[1]   P. Aerts, S. Kuypers, I. Genne, R. Leysen, J. Mewis, I. F. J. Vankelecom, P. A. Jacobs, J. Phys. Chem. B 110 (2006) 7425–7430.

[2]   *Separator membrane for alkaline electrolysis,* Zirfon® Pearl data sheet, AGFA.

[3]   J. Stojadinović, S. Weiss, F. La Mantia, Electrochim. Acta 127 (2014) 153–158.

DNA Sensing at femtomolar level using microfluidic electro-chemical cell: advantages of carbon-based transducers

B. Zribi,[1,2],* H. Korri-Youssoufi,[2] A. Ouerghi,[1] A. Cavanna,[1] A. Madouri,[1] A-M Haghiri-Gosnet[1]

[1]Laboratoire de Photonique et de Nanostructures, LPN UPR20, CNRS, route de Nozay, 91460 Marcousssis, France

[2]ICMMO, UMR-CNRS 8182, Bât 420, University Paris-Sud, 91460 Orsay, France

Abstract:

We report here a microfluidic multiplexed platform that integrates several electrochemical cells with a reduced volume at one hundred nanoliter scale capable of achieving ultrasensitive direct electrochemical detection of DNA. Our approach is based on the localized immobilization of DNA on carbon nanotubes in each microfluidic chamber by the electrochemical patterning method. Introduction of redox marker such as ferrocene between the biological receptor and the MWCNTs transducer allows measuring the charge transfer through current of redox signal. The hybridization reaction of immobilized single strand sequence from Hepatitis C virus and their complementary target (HCV virus) is used as biological model.

We demonstrate that this hybridization reaction in the confined space of the fluidic microchamber improves the sensitivity of the signal. Electrochemical DNA sensing in such microfluidic device allows direct detection at 0.1 femtomolar level. Compared to a bulk electrochemical cell featuring an identical biosensor and displaying a limit of detection of 1 picomolar, it corresponds to a decrease with four orders of magnitude. We envision that this microfluidic approach will find applications in the field of biosensing for practical devices for biology, medicine and environment.

Introduction:

The development of extremely sensitive, highly selective, simple, robust and yet inexpensive biosensing platforms is essential for a wide range of applications, including clinical diagnostics, environmental monitoring and food safety testing. Since accurate diagnostics need specific detection of very small amounts of DNA, there is a need to develop simple label-free DNA hybridization platforms with-out extensive sample pretreatments able to detect very low concentration below the femtomolar.

Microfluidics for the manipulation of small volumes of biological fluid is a tool of choice that allows multiplex analyses in independent micro-channels. Electrochemical detection appears as a gold start method for biosensors development since it gives direct sensitive measurement in real sample and is fully compatible with handheld systems (*Miodek et al, 2013*). Pairs of electrodes can be simply integrated into microchannels using conventional lithography processes (*Faure et al, 2014; Méance et al, 2014*). These electrochemical fluidic devices can thus be connected to handheld electronic readers giving access to portability and facility for their application in point of care system in diagnostic.

Biosensor design:

Electrochemical biosensors are composed of three essential parts: a **bioreceptor** (DNA, antibody, aptamer …), which is immobilized on the **transducer** working electrode, allowing molecular recognition with the molecular **target** (figure 1 left). For this study, we propose a new microfluidic platform for label-free DNA detection as a model to demonstrate the efficiency of the integration of electrochemical biosensors based on carbon-based materials in a microfluidic system. Carbon nanomaterials (CNTs and Graphene) have been chosen, since these materials exhibit extraordinary electrical properties. The mobility of charge carriers is sufficiently high ($\mu = 10^5$ cm^{2}V^{-1}s^{-1} for CNTs and $\mu = 2\ 10^5$ cm^{2}V^{-1}s^{-1} for graphene at 300 K), to promote fast charge transfer from the bioreceptor to the electrode and thus enhancing sensitivity. Concerning the CNTs, due to their large surface area (1315 m² g^{-1}) a large number of molecules can be electrografted or immobilized. Among different possible surface functionalization of the electrodes, we have used electrochemical patterning because this technique allows us to localize precisely the molecules only on the working electrode.

The hybridization reaction of immobilized single strand sequence from Hepatitis C virus and its complementary target (HCV virus) is used as biological model, which is monitored via direct electrochemical measurement of MWCNT-Fc redox properties in the microfluidic environment. Figure 1 (right) displays a schematic illustration of the biosensor based on modified ferrocene, as redox marker. After immobilization of the DNA probe, the complementary DNA target is detected through the direct measurement of the ferrocene redox signal. Moreover, the high specificity of hybridization is demonstrated by using the complementary and non-complementary DNA sequences.
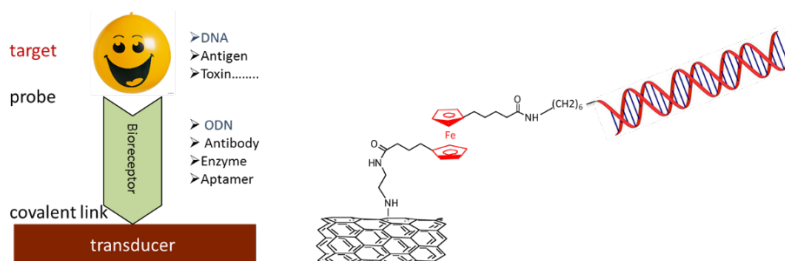

Figure 1: (left) general description of the electrochemical biosensor and (right) Schematic illustration of the biosensor based on MWCNTs-EDA-Fc-DNA for the detection of single-strand DNA virus from Hepatitis C (HCV Virus). The chemical pre-patterning is done inside each channel of the fluidic chip before the final hybridization step.

The covalent attachment of the ethylene diamine (EDA) molecules on the carbon transducer is "assisted" by electrochemical oxidation. This reaction is monitored by cyclic voltammetry (CV) by scanning the potential from -0.2 to -0.75 V (vs. Au) at a scan rate 200 mV·s^{-1} during 8 cycles in 7.4 mM EDA solution containing 0.5 M LiClO$_4$/ H$_2$O. This electrochemical oxidation

reaction produces radicals allowing covalent binding between ethylene diamine and the surface of the carbon transducer. In a second step, modified ferrocene, which is used as a redox marker, is covalently attached to the amine molecules. The remaining phtalimido ester groups of ferrocene ($Fc(NHP)_2$) will also serve for the covalent attachment of the DNA probe bearing amine group at the 5' terminal position. The electrical properties of each patterned layer (Au-MWCNT and Au-MWCNT-Fc(NHP)) after each functionalization step were examined with cyclic voltammetry and impedance spectroscopy (10 mM in KCl). Figure 2 (left) shows typical voltamograms obtained on MWCNTs macroelectrodes. Once the covalent attachment of ferrocene (redox marker), the appearance of characteristic redox signal is obtained at E~0.2 – 0.3 V. Finally, during the last step of surface functionalization, DNA probe is immobilized on the ferrocene (Figure 2 – right). At this step, the DNA bioreceptor covalently attached on the carbon-based transducer working electrode is ready for the last step of molecular recognition with the DNA target. The complementary DNA target is detected through the direct measurement of the ferrocene redox signal. Figure 2 (right) shows voltamograms recorded during hybridization with 3 different solutions of complementary DNA (1pM, 1nM and 1 μM).

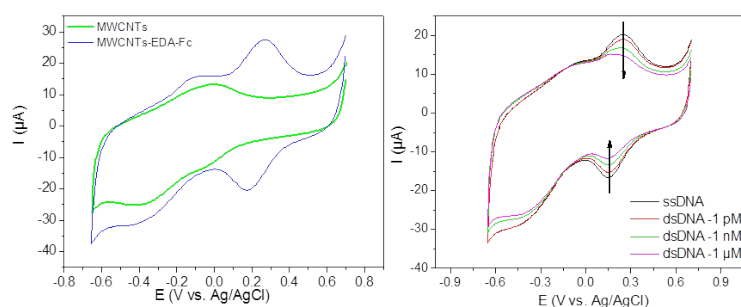*Figure 2: Characterization of biosensors using cyclic voltammetry on macroelectrodes ($S=1cm^2$). Cyclic voltamograms were recorded in a PBS phosphate buffer solution (10mM – pH=7.4) with a scan rate of 50mV/s – (left) during the preparation of the Au-MWCNTs-Fc for the 2 first steps of functionalization – (right) during the immobilization of the ssDNA probe and during the hydrization with different concentrations of complementary DNA target.*

After optimizing this functionalization on macro electrodes, similar experiments were implemented inside a microfluidic platform to study the role of confinement on the biosensor response. The microfluidic chip consists of a glass substrate with patterned gold electrodes, which is sealed with a 60μm–high polydimethylsiloxane (PDMS) cover that contains the fluidic channels and the detection chambers. Each electrochemical chamber of the microfluidic chip has a volume of around 300nL. The gold working microelectrodes are covered with modified MWCNTs. Similarly to our electrochemical study on macroelectrodes, cyclic voltammetry and impedance spectroscopy were used to analyze the different steps of functionalization and the hybridization. The microfluidic biosensor exhibits a dynamic range of detection from 0.1fM to 1pM whereas the dynamic range measured for conventional macro-cell is 1pM-100nM (Figure 3 (right)). A good reproducibility is observed with standard deviation of 1% for microfluidic cell. To check the specificity of the biosensing layer, similar experiments with non-complementary DNA strands have been performed. A decrease of around 11.5% in signal intensity was measured, which can be attributed to non-specific interaction of DNA on the surface of the microelectrode.
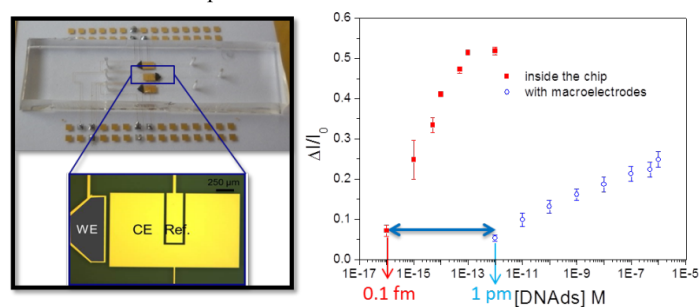

Figure 3: (left) Top view of the fluidic chip with 3 independent microchannels, each of them contianing one microelectrochemical chamber with 3 electrodes, and (right) the electrochemical calibration curves as function of DNA concentration deduced from both experiments on macroelectrodes (blue points) and microelectrodes inetgrated in the fluidic device (red points).

Conclusion: Compared to a conventional POC device with an amplification chamber, this new microfluidic platform holds the following advantages: (i) a very simple fabrication process for large scale production at low cost; (ii) a high quality biosensors operating under continuous flow conditions with a reduced volume of the biological reagents (< 1 μL); (iii) a reproducible direct ssDNA electrochemical biosensor with a limit of detection of 0.1 fM and a wide dynamic range from 0.1 fM to 1 pM.

References:
Miodek, A.; Castillo, G.; Hianik, T.; Korri-Youssoufi, H.; (2013) *Electrochemical Aptasensor of Human Cellular Piron Based on Multiwalled Carbon Nanotubes Modified with Dendrimers: A Platform for Connecting Redox Markers and Aptamers*, **Anal. Chem.**, 85, 7704-7712; Faure, M.; Pallandre, A.; Chebil, S.; Le Potier, I. ; Taverna, M.; Tribollet, B. ; Deslouis, C.; Haghiri-Gosnet, A-M.; Gamby, J. ; (2014) *Improved electrochemical detection of a transthyretin synthetic peptide in the nanomolar range with a two electrodes system integrated in a glass/PDMS microchip*, **Lab. Chip**., 14, 2800-2805 ; Méance, S.; Gamby, J.; Faure, M.; Kou, Q.; Haghiri-Gosnet, A-M.; (2014), *Electrochemiluminescence on a chip: towards à handheld electrically powered optofluidic source*, **Talanta**, 129, 150-154

A facile route to synthesize rutile TiO$_2$ nanorods arrays via hydro-thermal method

M. Guo[1, 2], Y. Gao[1], Q. Deng[3], X. Xia[1], G. Shao[2, 3*]

[1]Faculty of Materials Science and Engineering, Hubei University, Wuhan, 430062, P. R. China
[2]Institute for renewable energy and environmental technologies, University of Bolton, Bolton, BL3 5AB, UK
[3]UK-China Centre for Multifunctional Nanomaterials, Zhengzhou University, Zhengzhou 450001, China

Abstract: Hydrothermal method is a well-accepted sysnthesition method for its simple and low-cost procees as well as its rapid growth rate. Here highly-ordered, one-dimensional (1D) nanowires/nanorods arrays of rutile TiO2 were successfully grown on transparent, conductive glass substrate (FTO) by a hydrothermal method. Controllable length, diameter and density of the nanorod arrays (NRAs) were realized by adjusting hydrothermal conditions such as temperature, reaction time, concentration of reactants and type of solvent etc. The density of nanorods can be adjusted by varying the volume ratio of ethanol/water, and the orientation and crystallinity of TiO2 nanofilms were enhanced with increasing dosage of ethanol. Samples with ethanol as solvent displayed the best orientation and maximum thickness.

Keywords: self-assembly, TiO2 thin films, hydrothermal synthesis

Introduction

Nanostructural TiO2 has attracted considerable attentions due to its unique and excellent properties in optics, electronics, photochemistry and biology, as well as its applications in photovoltaic devices, light-emitting diodes (LEDs), photochemical dissociation of water, photocatalytic degradation of organic pollutants, lithium-ion batteries, gas sensing, DSSC, bacteriostasis etc[1-3]. Furthermore, vertically aligned, 1D film of semiconductor oxides (e.g. TiO2 nanotubes and ZnO nanowires) have been shown to enhance the efficiency of electron transport by increasing electron survivability. It is of great significance to explore a facile route for preparing single-crystalline 1D TiO2 nanomaterials with controllable phase composition and morphology to fulfil all kinds of applications. To date, many methods have been explored on one-dimensional TiO2 nanoarrays, including hydrothermal, template synthesis, electrochemical etching, chemical vapour deposition and sol–gel method. Among these methods, hydrothermal synthesis of TiO2 nanoarrays is a promising approach due to its simple process, low cost, facile and reproducible.[4,5] Many excellent work has been conducted to offer high-quality 1D TiO2 nanoarray films with hydrothermal treatment, but little information were given on the influence of hydrothermal parameters such as reaction temperature, reaction time, concentration of reactants and types of solvents etc. on rutile 1D TiO2 nanorods.[6,7] Thus, there is a requirement for us to systemic study how hydrother-mal parameters effect the morphology of ruitle films in details.

Ethanol was first introduced to prepared densely-packed nanowires which were vertically oriented grown on FTO glass substrate along the (110) crystal plane with a preferred (001) orientation by our team [4]. In this work, all the hydrothermal process were based on our previous work. The roles of hydrothermal conditions such as hydrothermal temperature, reaction time, concentration of reactants and kinds of solvent played were studied clearly. The morphologies, structures, orientation and optical properties of single-crystalline rutile TiO2 nanorod arrays (NRAs) were also investigated.

Experimental

Rutile nanorod synthetic process is the same as our previous work [4].The planar and cross-sectional morphology of the TiO2 nanorod thin films was characterized using field-emission-gun scanning electron microscopy (FE-SEM, Philips FEI XL30) at an accelerating voltage of 20 kV. Transmission electronmicroscopy (TEM) was carried out using a FEI Tecnai G2 microscope operated at 200 kV. And X-ray diffraction (XRD) was performed with a Bruker D8 X-ray diffractometer using the Cu Kα radiation (λ=1.5418 Å).

Results

Typical XRD patterns of films deposited on FTO substrate are presented in **Figure 1**. As we can see, the deposited films are pure rutile phase, all the position of the peaks appear upon agree well with tetragonal rutile phase (SG, P42/mnm; JCPDS No. 78-1508, a=b=0.4592 nm and c=0.2957 nm).[15] Compared to the standard powder diffraction patterns, the intensity ratio of peak (0 0 2)/(1 0 1) is significantly enhanced hence only this two peaks are visible while the other peaks including (1 1 0) and (1 1 1) are absent, which indicates that as-prepared films are highly oriented with respect to the substrate and TiO$_2$ films grow perpendicular to the substrate along the (1 1 0) crystal plane with a preferred (0 0 1) orientation. Also, the absence of these peaks strongly indicate that our nanfilms are single-crystal, agreeing with the previous work reported by our team.[4] These conclusions are confirmed by HRTEM results (vide infra).
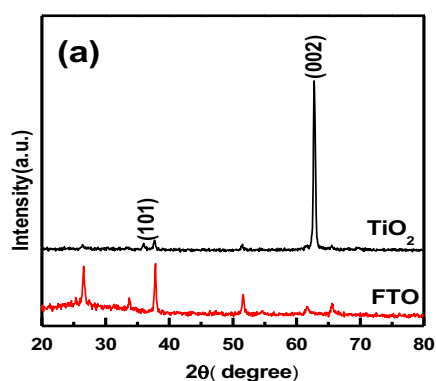
Figure 1 Typical XRD patterns of Rutile nanorods: The sample was prepared at 180℃, 4h, with ethanol/water ratio 1:1.

Figure 2 illustrates corresponding FESEM and HRTEM images of TiO₂ films. According to our previous report, for the ethanol volume at 15 ml (50% of total solvent volume), completely dense packed thin films composed of thin nanowires/ nanorods were achieved, and all NARs (nanorods) are remarkable dense films and it is uniformly aligned with single thinner nanowires in average diameters. The results are further proved in the following text. *Figure 2 Morphology of typical rutile nanorod. The*
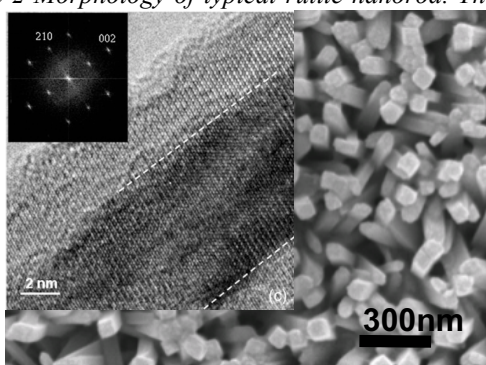
density of the nanorod varies with the volume ratio of ethano/water. HRTEM image exhibits high crystalinity of the nanorods, which contained clomnar subgrain boundaries. Inset shown corresponding FFT from the top subgrain.

The HRTEM image and FFT transform of selected area are well consisted with XRD results.The corresponding FFT from the rod is consisted with the single crystal diffraction pattern of the [001] longitudinal direction, which confirms the results of XRD.

Various hydrothermal times were taken into account to study the time dependent growth process with results displayed in Fig. 5. All samples were obtained at 180℃ using 15ml ethanol as the solvent. As illustrated in Fig. 5, the intensity ratio of peak (002) /(101) increased from 1h to 4hrs, which reveals that crystallinity and the degree of orientation become better with time prolonged. Meanwhile,the intensity ratio is almost the same for sample prepared for 2hrs and 4hrs, which indicated that the

main nucleation and crystallization process of TiO2 rods were already accomplished in the first 2 hours, while in the later 2hrs, the improvement of film quality and increase of film thickness are the dominate process. when growth time extended over 24 h, a white film composed of aligned TiO2 nanorods starts to dissolve into the solution and peel off the FTO substrate, same phenomenon were reported by ref.6 . It's concluded that in the 1st hour, an initial layer of short and coarse rutile polycrystalline seed grow random on the FTO substrate; in the next few hours, rutile TiO2 nucleated on the crystal seeds, achieve the orientation process, and increase the thickness of the film.
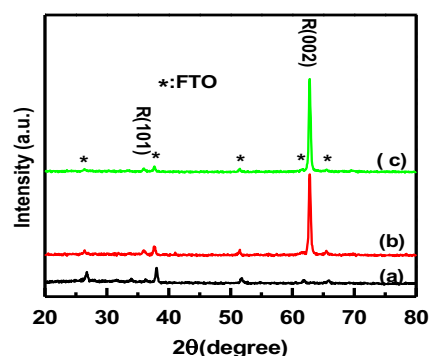

Figure 3 XRD results of Rutile nanorods prepared for different time.(a) 1h; (b) 2h; (c) 4h.

Conclusion

Single-crystal rutile TiO2 nanorod has been successfully synthetized on FTO substrate by hydrothermal method. The hydrothermal growth time was discussed to get better understand on hydrothermalnucleation. Results show that the orientation takes place in the first 2 hour and the length increases greatly whiel maintain good crystallization and degree of orientation above 2 hrs.

[1] Chuncheng Chen, Wanhong Ma, Jincai Zhao. Chem Soc Rev 2010; 39: 4206–4219.
[2] Dorian A. H. Hanaor, Charles C. Sorrell. J. Mater. Sci. 2011; 46:855–874
[3] Weijia Zhou, Hong Liu, Robert I. Boughton, Guojun Du, Jianjian Lin, Jiyang Wang, Duo Liu. J. Mater. Chem. 2010; 20: 5993–6008
[4] Y. Zhang, Y. Gao, X.H. Xia, Q.R. Deng, M.L. Guo, L. Wan, G. Shao. Materials Letters 2010; 64: 1614–1617
[5] Xinjian Feng, Karthik Shankar, Oomman K. Varghese, Maggie Paulose, Thomas J. Latempa, and Craig A. Grimes. Nano Lett 2008; 8: 3781-3786.
[6] B. Liu, E.S. Aydil. J. Am. Chem. Soc. 2009, 131 3985.
[7] Hong-En Wang, Zhenhua Chen, Yu Hang Leung, Chunyan Luan, Chaoping Liu, Yongbing Tang, Ce Yan, Wenjun Zhang, Juan Antonio Zapien, Igor Bello, Shuit-Tong Lee. Applied Physics Letters 2010; 96: 263104.